ISSN 0021-8944, Journal of Applied Mechanics and Technical Physics, 2016, Vol. 57, No. 1, pp. 117–126. © Pleiades Publishing, Ltd., 2016.
Original Russian Text © J. Alinejad.

LATTICE BOLTZMANN SIMULATION OF A FLUID FLOW AROUND A TRIANGULAR UNIT OF THREE ISOTHERMAL CYLINDERS

J. Alinejad

UDC 532.5, 533.6

Abstract: The lattice Boltzmann method is employed to simulate heat transfer in the flow past three arrangements of elliptical and circular cylinders under an isothermal boundary condition. The lattice Boltzmann equations and the Bhatnagar–Gross–Krook model are used to simulate two-dimensional forced convection at $30 \leqslant \mathrm{Re} \leqslant 100$ and $\mathrm{Pr} = 0.71$. Pressure distributions, isotherms, and streamlines are obtained. Vortex shedding maps are observed in detail for several cases. The present results are in good agreement with available experimental and numerical data.

Keywords: lattice Boltzmann model, isothermal cylinders, vortex shedding, Reynolds number.

DOI: 10.1134/S0021894416010132

INTRODUCTION

The problem of forced convection in fluid flows past cylinders of various cross sections has been a challenge for both theoretical and applied investigations [1–3]. Bluff body flows constitute an important class of problems within the domain of fluid mechanics. An elliptical cylinder is one of the important bluff objects referred in computational fluid dynamics (CFD) in which the aspect ratio and the angle of attack are important parameters [4]. It is also known that elliptical cylinders offer a smaller flow resistance and higher heat transfer rates than circular cylinders. In recent decades, the lattice Boltzmann method (LBM) has proved its capability of simulating a large variety of fluid flows. For isothermal fluid flows, the LBM was found to be an accurate, stable, and computationally economic method compared to the classical CFD methods [5]. The thermal LBM model was first investigated by Massaioli et al. [6]. The main limitation of using the LBM in engineering applications is the lack of a satisfactory model for thermal fluid flow problems. A multi-speed approach consists in extending the distribution function in order to obtain the macroscopic temperature [7, 8]. However, this approach requires much more computational effort because of the additional discrete speeds and suffers from numerical instabilities. An alternative approach consists in finding the velocity by the LBM and solving the macroscopic temperature equation independently. The coupling to the LBM is made by adding a potential to the distribution function equation [9, 10]. Korichi and Oufer [11] carried out a numerical investigation of the flow field and heat transfer enhancement in a channel containing three obstacles: two attached to the lower wall and one to the upper wall. The results showed that the transition from a steady to an unsteady flow occurs at lower values of the Reynolds number as compared to a channel with obstacles attached only to the lower wall. A study of a steady flow around two circular cylinders in a tandem arrangement at four different Prandtl numbers ($\mathrm{Pr} = 0.1$, 1.0, 10.0, and 100.0) was reported recently by Juncu [12]. Numerical simulations of a forced convective incompressible flow in a horizontal plane channel and heat transfer over two isothermal tandem square cylinders were carried out by Farhadi et al. [13] and Mohammadi et al. [14] by using the

Department of Mechanical Engineering, Sari Branch, Islamic Azad University, Sari, Iran; Alinejad_javad@iausari.ac.ir. Translated from Prikladnaya Mekhanika i Tekhnicheskaya Fizika, Vol. 57, No. 1, pp. 136–145, January–February, 2016. Original article submitted January 10, 2013; revision submitted January 24, 2014.

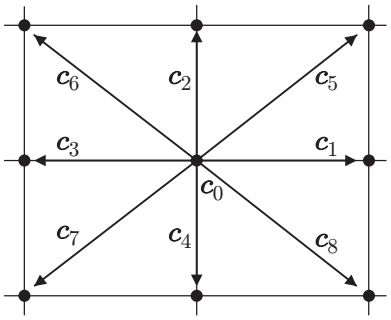

Fig. 1. Nine-velocity lattice model.

finite volume and LBM methods. Their study revealed the effects of the gap between two cylinders, the Reynolds number ranging within Re = 100–1000, and the blockage ratio on the characteristics of the flow field and heat transfer. The present study emphasizes the implementation of the LBM for simulating the flow field and heat transfer around isothermal cylinders to compare its results with results obtained by the finite element solution of the Navier–Stokes equations. The simulation is conducted at $\mathrm{Pr} = 0.71$ and $30 \leqslant \mathrm{Re} \leqslant 100$.

1. LATTICE BOLTZMANN METHOD

The lattice Boltzmann method was developed as an alternative numerical approach for solving a wide class of gas-dynamic problems [15–17].

1.1. Governing Equation

The LBM is derived from lattice gas methods and can be regarded as a first-order explicit discretization of the Boltzmann equation in the phase space. The LBM is a powerful numerical technique for simulating fluid flows [15, 18, 19] and heat transfer [20, 21]. In contrast to the classical macroscopic Navier–Stokes (NS) approach, the lattice Boltzmann method uses a mesoscopic simulation model to simulate the fluid flow [20]. It uses modeling of the movement of fluid particles to capture macroscopic fluid quantities, such as velocity and pressure. In this approach, the fluid domain is made discrete in uniform Cartesian cells, each containing a fixed number of distribution functions that represent a certain number of fluid particles moving in these discrete directions. Hence, depending on the dimension and number of velocity directions, there are different models that can be used. The present study deals with a two-dimensional flow and a two-dimensional square lattice with nine velocities. The velocity vectors $\boldsymbol{c}_0, \ldots, \boldsymbol{c}_8$ of the D2Q9 model are shown in Fig. 1. For each velocity vector, the particle distribution function is stored. The velocities of the D2Q9 model (see Fig. 1) are calculated by the formulas

$$\boldsymbol{c}_k = \begin{cases} (0,0), & k = 0, \\ (\pm 1, 0)c, (0, \pm 1)c, & k = 1,2,3,4, \\ (\pm 1, \pm 1)c, & k = 5,6,7,8, \end{cases}$$

where $c = \Delta x/\Delta t$ and k is the lattice velocity direction.

The LBM model used in the present work is the same as that employed in [20]. The distribution functions are calculated by solving the lattice Boltzmann equation. After introducing the Bhatnagar–Gross–Krook (BGK) approximation, the Boltzmann equation can be formulated as follows [22]:

$$f_k(x + \boldsymbol{c}_k\,\Delta t, t + \Delta t) = f_k(x,t) + \frac{\Delta t}{\tau}\,[f_k^{\mathrm{eq}}(x,t) - f_k(x,t)].$$

Here Δt denotes the lattice time step, c_k is the discrete lattice velocity in the direction k, τ denotes the lattice relaxation time, and f_k^{eq} is the equilibrium distribution function corresponding to the lattice velocity $\boldsymbol{c}_k$ and calculated by the formula

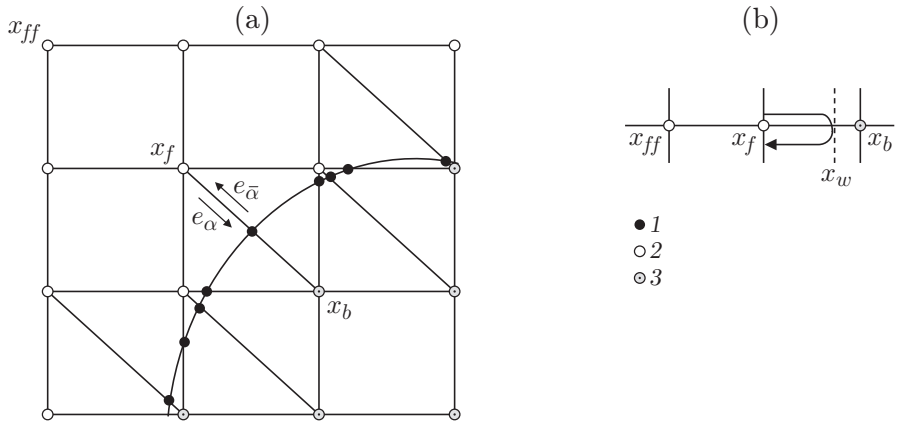

Fig. 2. Distribution of nodes near the curved boundary (a) and the bounce-back with interpolation after the collision (b): nodes on the boundary x_w (*1*), boundary nodes in the fluid region x_f (*2*), and boundary nodes in the solid body region x_b (*3*).

$$f_k^{\mathrm{eq}} = \omega_k \rho \Big(1 + \frac{\boldsymbol{c}_k \cdot u}{c_s^2} + \frac{1}{2}\,\frac{(\boldsymbol{c}_k \cdot \boldsymbol{u})^2}{c_s^4} - \frac{1}{2}\,\frac{\boldsymbol{u}^2}{c_s^2}\Big), \tag{1}$$

where $\omega_k = 4/9$ for $k = 0$, $\omega_k = 1/9$ for $k = 1, 2, 3$, and 4, $\omega_k = 1/36$ for $k = 5, 6, 7$, and 8, and $c_s = c_k/\sqrt{3}$ is the lattice speed of sound. The macroscopic fluid variables (density and velocity) are computed as the first two moments of the distribution functions for each cell [22]:

$$\rho = \sum_{k=0}^{8} f_k, \qquad \boldsymbol{u} = \frac{1}{\rho}\sum_{k=0}^{8} f_k \boldsymbol{c}_k. \tag{2}$$

For the temperature field, the distribution of g has the form

$$g_k(x + \boldsymbol{c}_k\,\Delta t, t + \Delta t) = g_k(x,t) + \frac{\Delta t}{\tau_g}\,[g_k^{\mathrm{eq}}(x,t) - g_k(x,t)].$$

The corresponding equilibrium distribution functions for the fluid and solid, respectively, are defined as follows [18]:

$$g_k^{\mathrm{eq}} = \omega_k T \Big(1 + \frac{\boldsymbol{c}_k \cdot \boldsymbol{u}}{c_s^2}\Big), \qquad g_k^{\mathrm{eq}} = \omega_k T.$$

The temperature field is computed as

$$T = \sum g_k.$$

1.2. Curved Boundary Treatment

Let us consider the geometry of a part of an arbitrary curved wall (Fig. 2). To impose the no-slip boundary condition, it is necessary to define the function $f(x_b, t)$. The fraction of the fluid Δ in the cell intersected by the boundary is

$$\Delta = \frac{\|x_f - x_w\|}{\|x_f - x_b\|}.$$

The standard (half-way) bounce-back no-slip boundary condition always assumes that $\Delta = 0.5$ on the boundary wall. Due to the curved boundaries, the values in the interval $\Delta = 0$–1 are possible. Figure 2b shows the bounce-back behavior at $\Delta < 0.5$. The reflected distribution function $f_a(x, t + \Delta t)$ at x_f is unknown. The fluid particles in the LBM are always considered to move by one cell length per time step. In order to calculate the reflected distribution function in the node x_f, the interpolation scheme [23] was applied. To calculate the distribution function in the solid region $f_a(x_b, t)$, the bounce-back boundary conditions were combined with interpolations including a one-half grid spacing correction at the boundaries. Then, the Chapman–Enskog expansion for the post-collision distribution function takes the form

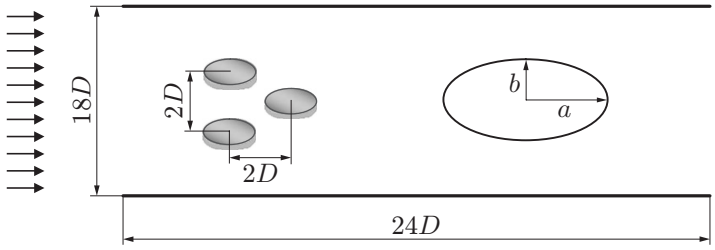

Fig. 3. Schematic diagram of the computational domain.

$$\tilde{f}_{\bar{\alpha}}(x_b, t+\Delta t) = (1-\lambda)\tilde{f}_{\alpha}(x_f, t+\Delta t) + \lambda f^0_{\alpha}(x_b, t+\Delta t) - 2\,\frac{3}{c^2}\,w_{\alpha}\rho(x_f, t+\Delta t)e_{\alpha}u_w,$$

where

$$f^0_{\alpha}(x_b, t+\Delta t) = f^{\mathrm{eq}}_{\alpha}(x_f, t+\Delta t) + \frac{3}{c^2}\,w_{\alpha}\rho(x_f, t+\Delta t)e_{\alpha}(u_{bf} - u_f),$$

$$u_{bf} = u_{ff}, \quad \lambda = \frac{2\Delta - 1}{\tau_m - 2} \quad \text{for} \quad 0 < \Delta \leqslant \frac{1}{2},$$

$$u_{bf} = \Big(1 - \frac{3}{2\Delta}\Big)u_f + \frac{3}{2\Delta}\,u_w, \quad \lambda = \frac{2\Delta - 1}{\tau_m + 1/2} \quad \text{for} \quad \frac{1}{2} < \Delta \leqslant 1.$$

1.3. Force and Heat Transfer Evaluation

Heat transfer between hot and cold walls was computed by using the local and mean Nusselt numbers:

$$\mathrm{Nu}_l = -\frac{\partial T}{\partial n}\Big|_{wall}, \qquad \mathrm{Nu}_m = \frac{1}{2\pi}\int\limits_0^{2\pi} \mathrm{Nu}_l\; d\theta.$$

The drag coefficient and the pressure coefficient are defined as

$$C_D = \frac{F_D}{\rho U^2_{\infty} D/2}, \qquad C_P = \frac{P - P_{\infty}}{\rho U^2_{\infty}/2}.$$

1.4. Numerical Procedure

The physical geometry considered in this study is shown in Fig. 3. The cylinders are arranged in a triangular configuration. This triangular configuration is mounted inside a channel, which is sufficiently wide in a way that its walls exert no measurable effect on the flow field characteristics. Moreover, the cylinders are assumed to be sufficiently long so that the ends effects are neglected. The temperature of the walls T_c is equal to the temperature of the incoming fluid T_{∞}, which is constant during the computation. The temperature of the cylinders surfaces T_h is also assumed to be constant; however, it is higher than the incoming fluid temperature.

In this study, three kinds of boundary conditions are applied: the bounce-back condition is imposed on the surfaces of the cylinders and channel walls, and constant velocity and constant pressure are set at the inlet and outlet boundaries. The bounce-back boundary condition has the form

$$f_7(x, t+\Delta t) = f_5(x,t), \qquad f_4(x, t+\Delta t) = f_2(x,t), \qquad f_8(x, t+\Delta t) = f_6(x,t)$$

on the upper wall of the channel and

$$f_5(x, t+\Delta t) = f_7(x,t), \qquad f_2(x, t+\Delta t) = f_4(x,t), \qquad f_6(x, t+\Delta t) = f_8(x,t)$$

on the lower wall of the channel.

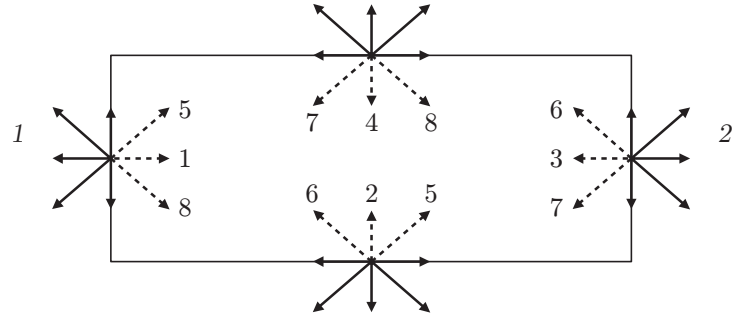

Fig. 4. Distribution functions at the computational domain boundaries: channel inlet (*1*) and channel outlet (*2*).

At the inlet of the channel, the boundary condition with a known velocity u_{in} is applied (Fig. 4), and three unknown distribution functions are calculated on the basis of Eq. (2):

$$\rho_{\text{in}} = f_0 + f_1 + f_2 + f_3 + f_4 + f_5 + f_6 + f_7 + f_8,$$

$$\rho_{\text{in}} u_{\text{in}} = f_1 + f_5 + f_8 - f_3 - f_6 - f_7;$$

$$f_1 - f_1^{\text{eq}} = f_3 - f_3^{\text{eq}}. \tag{3}$$

It should be noted that Eq. (3) follows from the equilibrium condition normal to the boundary, where f^{eq} can be calculated from Eq. (1) as

$$f_1^{\text{eq}} = \frac{1}{9}\,\rho_{\text{in}}\Big(1 + 3u_{\text{in}} + \frac{9}{2}\,u_{\text{in}}^2 - \frac{3}{2}\,u_{\text{in}}^2\Big); \tag{4}$$

$$f_3^{\text{eq}} = \frac{1}{9}\,\rho_{\text{in}}\Big(1 - 3u_{\text{in}} + \frac{9}{2}\,u_{\text{in}}^2 - \frac{3}{2}\,u_{\text{in}}^2\Big). \tag{5}$$

Substituting Eqs. (4) and (5) into Eq. (3), we obtain

$$f_1 = f_3 + (2/3)\rho_{\text{in}} u_{\text{in}}.$$

Solving these equations, we find the remaining unknown distribution functions:

$$\rho_{\text{in}} = \frac{(f_0 + f_2 + f_4) + 2(f_3 + f_7 + f_6)}{1 - u_{\text{in}}},$$

$$f_5 = f_7 - \frac{1}{2}\,(f_2 - f_4) + \frac{1}{6}\,\rho_{\text{in}} u_{\text{in}}, \qquad f_8 = f_6 + \frac{1}{2}\,(f_2 - f_4) + \frac{1}{6}\,\rho_{\text{in}} u_{\text{in}}.$$

At the channel outlet, the open boundary condition is imposed. The applied approach is to assume that the pressure at this boundary, i.e., the density ρ_{out}, is known. Three unknown distribution functions are calculated as

$$u_x = -1 + \frac{(f_0 + f_2 + f_4) + 2(f_1 + f_5 + f_8)}{\rho_{\text{out}}},$$

$$f_3 = f_1 - \frac{2}{3}\,\rho_{\text{out}} u_x, \quad f_7 = f_5 + \frac{1}{2}\,(f_2 - f_4) - \frac{1}{6}\,\rho_{\text{out}} u_x, \quad f_6 = f_8 - \frac{1}{2}\,(f_2 - f_4) - \frac{1}{6}\,\rho_{\text{out}} u_x.$$

1.5. Code Validation

The numerical simulation was performed by an in-house code written in FORTRAN, by using the LBM. Numerical investigations were carried out for the flow past a single circular cylinder confined in a channel. Comparisons of pressure distributions and drag coefficients obtained in the present work for $\text{Re} = 100$ with the previous works [24–28] show that very good agreement has been obtained (Fig. 5 and Table 1).

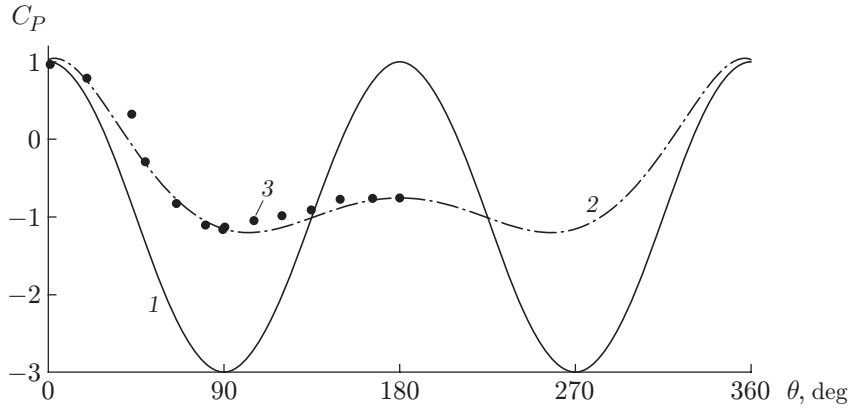

Fig. 5. Pressure distribution on the circular cylinder surface: potential flow (*1*), LBM solution for Re = 100 (*2*), and experimental data [2] for Re = 100 (*3*).

Table 1. Drag coefficient C_D for a circular cylinder at Re = 100

Reference	C_D	Reference	C_D
Present study	1.45	Khan et al. [26]	1.40
Park et al. [24]	1.33	Hoffman [27]	1.47
Sucket and Brauer [25]	1.45	Von Wieselsberger [28]	1.43

Table 2. Mean Nusselt numbers for different arrangements of the cylinders

Arrangement of the cylinders	Nu_m		
	Cylinder 1	Cylinder 2	Cylinder 3
Fig. 7a	6.30	6.39	5.81
Fig. 7b	5.65	5.66	5.15
Fig. 7c	6.24	6.29	6.08

2. RESULTS AND DISCUSSION

The streamline patterns for different Reynolds numbers are shown in Fig. 6. For low Reynolds numbers (Re < 60), the streamlines are steady and agree well with previous experimental results. At Re > 60, the streamlines vary due to flow unsteadiness. As the Reynolds number increases, the wake region decreases, which offers a qualitative explanation for the decrease in the drag coefficient on the cylinder surface. At low Reynolds numbers, it is seen that two vortices downstream of the cylinder, symmetrically placed about the channel centerline, remain attached to the cylinder. The size of the vortices for the circular cylinder is greater than those for the elliptical one and increases with the Reynolds number. If the Reynolds number is increased beyond a certain critical value, the streamline patterns on the rear side of the cylinder become wavy and sinuous, and unsteady vortex shedding becomes more visible. Figure 6 depicts the streamline patterns for the flow past the circular and elliptical cylinders at different Reynolds numbers. Steady flow vortices seem to be more and more elongated as the Reynolds number increases. It is seen from Fig. 6 that the vortices are shed at Re = 100, which is known as the famous von Kármán vortex street.

The distributions of the local Nusselt number and isotherms at Re = 50 are presented in Fig. 7. It is seen that the flow near the downstream cylinder faces is accelerated, the streamline patterns become wavy, and the unsteady vortex shedding pattern becomes more visible. The maximum Nusselt number of each cylinder occurs at the stagnation point (Figs. 7a, 7c, and 7e). At a fixed Reynolds number, the maximum local heat transfer rates on the surfaces of the elliptical cylinders are significantly higher than those on the surfaces of the circular cylinders. The mean Nusselt numbers for different arrangements of the cylinders are listed in Table 2. It is clear that the value

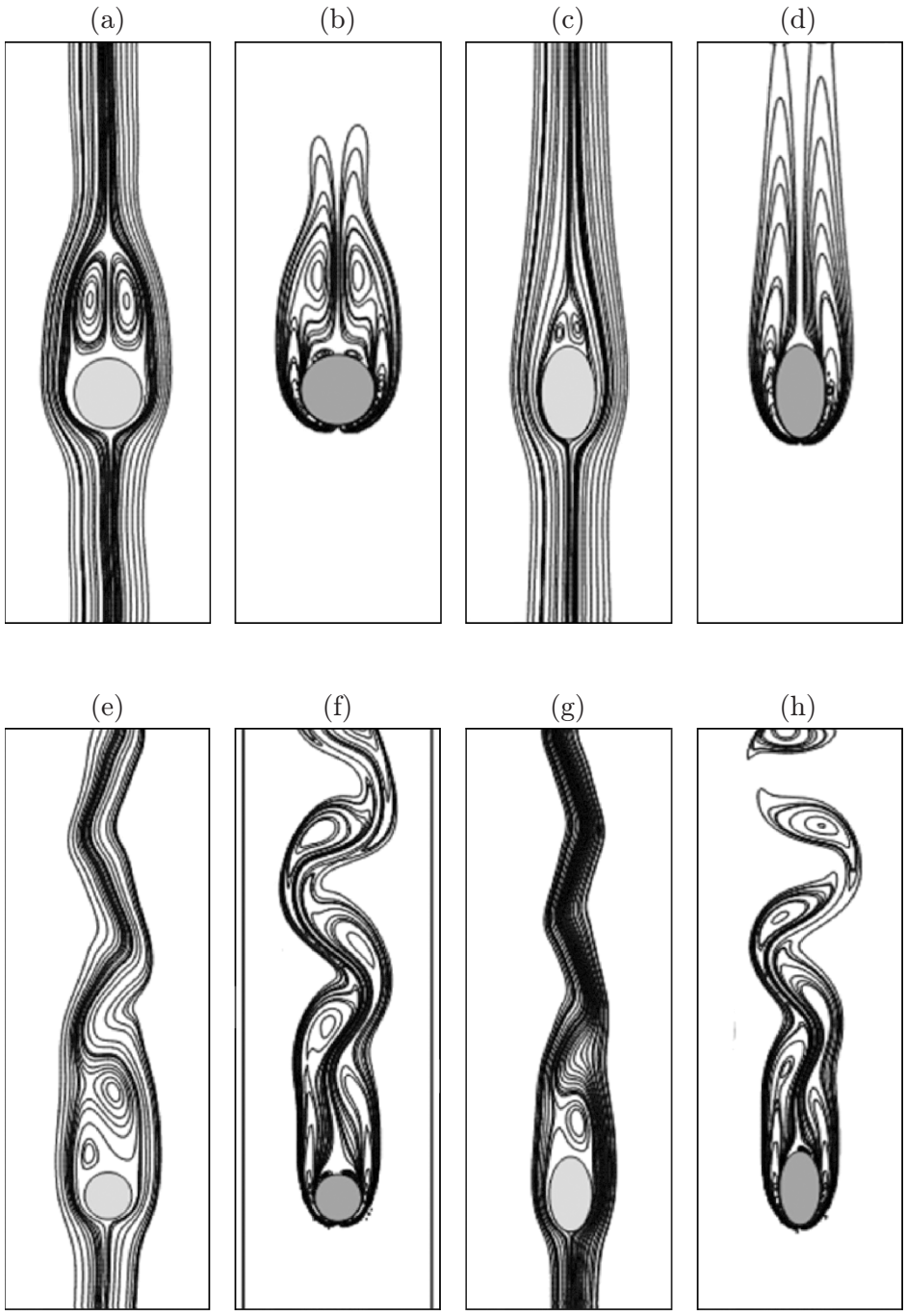

Fig. 6. Streamline patterns for steady flows behind a circular cylinder (a, b, e, and f) and behind an elliptical cylinder (c, d, g, and h) at different Reynolds numbers: Re = 30 (a–d) and 100 (e–h).

of Nu_m is lower for the downstream cylinders. The Nusselt numbers for the circular cylinders are found to be lower than for any geometry considered in this study; the presence of a vertical elliptical cylinder further downstream leads to an increase in the rate of convective heat transfer from the hot cylinder.

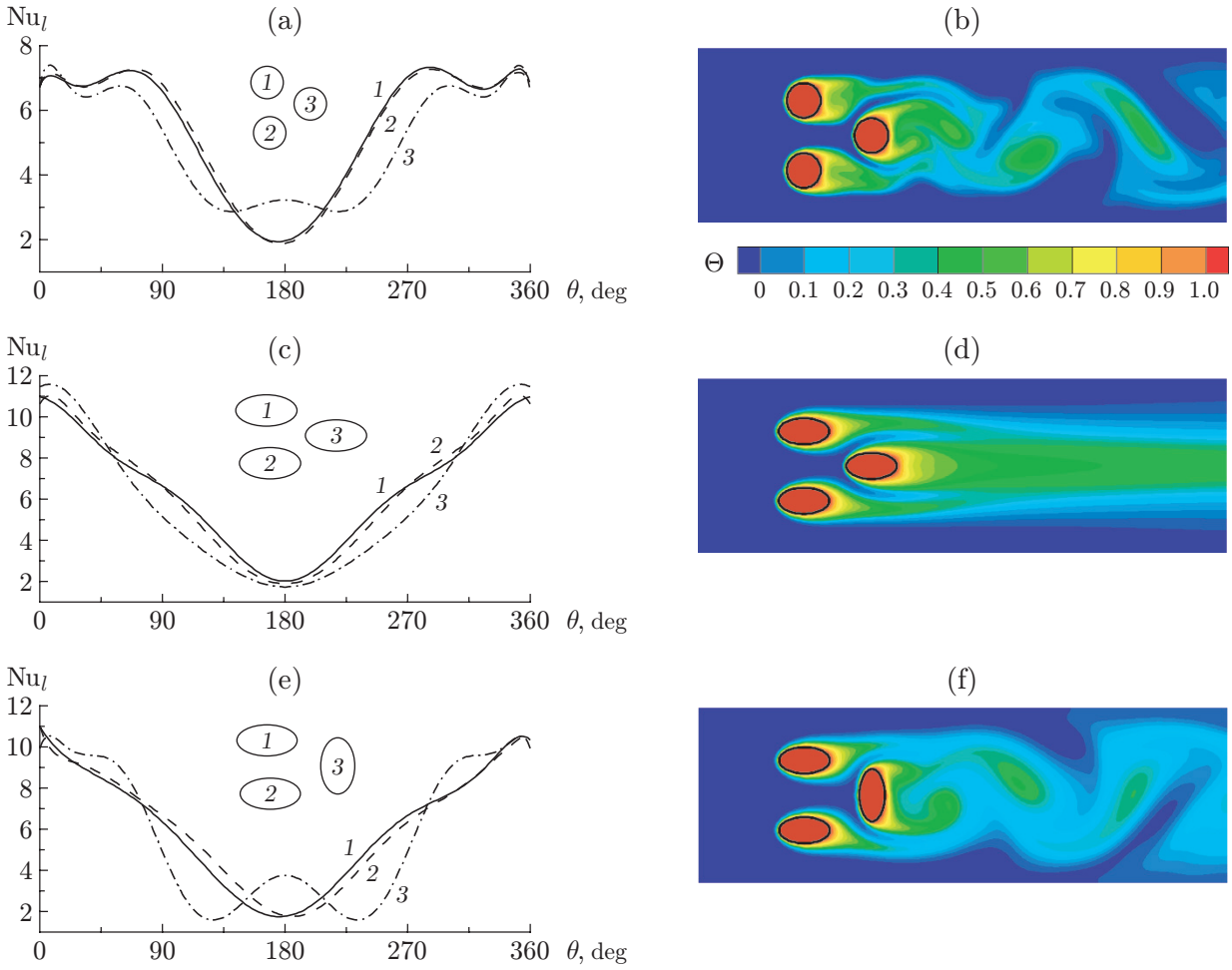

Fig. 7. Distributions of the local Nusselt number (a, c, and e) and isotherms (b, d, and f) for different shapes and arrangement of the cylinders at Re = 50: circular cylinders (a and b); elliptical cylinders (c–f); the cylinders are denoted by the numbers *1–3*.

CONCLUSIONS

A detailed numerical study of the flow and heat transfer around a triangular unit of three isothermal cylinders with different arrangements was investigated. A two-dimensional lattice Boltzmann method (LBM) was developed to study heat transfer problems. In comparison with conventional CFD methods, the LBM has a simple calculation procedure and can be used to describe complex geometries and boundary conditions. To illustrate the flexibility of the method, various parameters, such as the pressure distribution and the drag coefficient, were investigated. It was shown that these results were in good agreement with previous results.

In conclusion, some of the main points are briefly remarked.

The LBM can reproduce the essential features of the flow past a cylinder.

The maximum rate of heat transfer of the triangular unit is reached at the stagnation point of the cylinder.

The mean Nusselt number of upstream cylinders is higher in comparison to the downstream cylinder.

The local rates of heat transfer at the elliptical cylinders are significantly higher than those on the surfaces of the circular cylinders.

The presence of a vertical elliptical cylinder further downstream leads to an increase in the rate of convective heat transfer from the hot cylinder.

REFERENCES

1. R. Mittal and S. Balachandar, "Direct Numerical Simulation of Flow Past Elliptic Cylinders," J. Comput. Phys. **124**, 351–367 (1996).
2. B. Sharman, F. S. Lien, L. Davidson, and C. Norberg, "Numerical Predictions of Low Reynolds Number Flows over Two Tandem Circular Cylinders," Int. J. Numer. Methods Fluids **47**, 423–447 (2005).
3. D. Arumuga Perumal, G. V. S. Kumar, and A. K. Dass, "Lattice Boltzmann Simulation of Viscous Flow Past Elliptical Cylinder," J. CFD Lett. **4**, 127–139 (2012).
4. K. Shintani, A. Umemura, and A. Takano, "Low-Reynolds-Number Flow Past an Elliptic Cylinder," J. Fluid Mech. **136**, 277–289 (1983).
5. F. J. Higuera and J. Jimenez, "Boltzmann Approach to Lattice Gas Simulation," Europhys. Lett. **9**, 663–668 (1989).
6. F. Massaioli, R. Benzi, and S. Succi, "Exponential Tails in Two-Dimensional Rayleigh–Be'nard Convection," Europhys. Lett. **21**, 305–310 (1993).
7. Y. Chen, H. Ohashi, and M. A. Akiyama, "Thermal Lattice Bhatnagar–Gross–Krook Model without Nonlinear Deviations in Macro Dynamic Equations," Phys. Rev. E **50**, 2776–2783 (1994).
8. P. Pavlo, G. Vahala, L. Vahala, and M. Soe, "Linear-Stability Analysis of Thermo-Lattice Boltzmann Models," J. Comput. Phys. **139**, 79–91 (1998).
9. B. Crouse, M. Krafczyk, S. Kuhner, et al., "Indoor Air Flow Analysis Based on Lattice Boltzmann Methods," Energy Build **34**, 941–949 (2002).
10. A. D'Orazio, M. Corcione, and G. P. Cielata, "Application to Natural Convection Enclosed Flows of a Lattice Boltzmann BGK Model Coupled with a General Purpose Thermal Boundary Condition," Int. J. Thermal Sci. **43**, 575–586 (2004).
11. A. Korichi and L. Oufer, "Numerical Heat Transfer in a Rectangular Channel with Mounted Obstacles on the Upper and Lower Walls," Int. J. Thermal Sci. **44**, 644–655 (2005).
12. G. Juncu, "A Numerical Study of Momentum and Forced Convection Heat Transfer Around Two Tandem Circular Cylinders at Low Reynolds Numbers. Pt 2. Forced Convection Heat Transfer," Int. J. Heat Mass Transfer **50**, 3799–3808 (2007).
13. M. Farhadi, K. Sedighi, and M. M. Madani, "Convective Cooling of Tandem Heated Squares in a Channel," J. Mech. Eng. Sci. **223**, 965–978 (2009).
14. M. Mohammadi Pirouz, M. Farhadi, K. Sedighi, et al., "Lattice Boltzmann Simulation of Conjugate Heat Transfer in a Rectangular Channel with Wall-Mounted Obstacles," J. Sci. Iranica B **18**, 213–222 (2011).
15. B. Chopard and P. O. Luthi, "Lattice Boltzmann Computations and Applications to Physics," Theoret. Comput. Phys. **217**, 115–130 (1999).
16. R. R. Nourgaliev, T. N. Dinh, T. G. Theofanous, and D. Joseph, "The Lattice Boltzmann Equation Method: Theoretical Interpretation, Numerics and Implications," Int. J. Multiphase Flow **29**, 117–169 (2003).
17. D. Yu, R. Mei, L. S. Luo, and W. Shyy, "Viscous Flow Computations with the Method of Lattice Boltzmann Equation," Progr. Aerospace Sci. **39**, 329–367 (2003).
18. A. A. Mohammad, *Applied Lattice Boltzmann Method for Transport Phenomena Momentum Heat Mass Transfer* (Univ. Calgary Press, Calgary, 2007).
19. D. M. Aghajani, M. Farhadi, and K. Sedighi, "Effect of Heater Location on Heat Transfer and Entropy Generation in the Cavity Using the Lattice Boltzmann Method," Heat Transfer Res. **40**, 521–536 (2009).
20. A. Mezrhab, M. Jami, C. Abid, et al., "Lattice Boltzmann Modeling of Natural Convection in an Inclined Square Enclosure with Partitions Attached to its Cold Wall," Int. J. Heat Fluid Flow **27**, 456–465 (2006).
21. X. He and L. S. Luo, "Lattice Boltzmann Model for the Incompressible Navier–Stokes Equations," J. Statist. Phys. **88**, 927–944 (1997).
22. N. Thürey and U. Rüde, "Stable Free Surface Flows with the Lattice Boltzmann Method on Adaptively Coarsened Grids," Comput. Visual. Sci. **12**, 247–263 (2009).

23. Z. L. Guo, Ch. Zheng, and B. C. Shi, "An Extrapolation Method for Boundary Conditions in Lattice Boltzmann Method," Phys. Fluids **14** (6), 2007–2010 (2002).
24. J. Park, K. Kwon, and H. Choi, "Numerical Solutions of Flow Past a Circular Cylinder at Reynolds Number up to 160," KSME Int. J. **12**, 1200 (1998).
25. D. Sucker and H. Brauer, "Fluiddynamikbei der Angestromten Zilindern," Wärme- und Stoffübertrag **8**, 149 (1975).
26. W. A. Khan, J. R. Culham, and M. M. Yovanovich, "Fluid Flow Around and Heat Transfer from Elliptical Cylinders: Analytical Approach," J. Thermophys. Heat Transfer **19**, 178–185 (2005).
27. J. Hoffman, "Efficient Computation of Mean Drag for the Subcritical Flow Past a Circular Cylinder using General Galerkin G2," Int. J. Numer. Methods Fluids **59** (11), 1241–1258 (2009).
28. C. Von Wieselsberger, "Neuere Festellungen über die Gesetze des Flüssigkeits un Luftwiderstands," Phys. Z. **22**, 321–328 (1921).